Applied Catalysis B: Environmental 324 (2023) 122244

Contents lists available at ScienceDirect

Applied Catalysis B: Environmental

journal homepage: www.elsevier.com/locate/apcatb

DFT calculation screened CoCu and CoFe dual-atom catalysts with remarkable hydrogen evolution reaction activity

Mingyang Jiao [a,b], Zhipeng Chen [c], Nailiang Wang [d], Licheng Liu [a,b,*]

[a] Qingdao Institute of Bioenergy and Bioprocess Technology, Chinese Academy of Sciences, Qingdao 266101, Shandong, China
[b] Shandong Energy Institute, Qingdao 266101, Shandong, China
[c] School of Chemistry and Chemical Engineering, Anhui University of Technology, Ma'anshan 243032, China
[d] State Key Laboratory of High-efficiency Utilization of Coal and Green Chemical Engineering, Yinchuan, Ningxia 750021, China

ARTICLE INFO

Keywords:
Dual-atom catalysts
DFT calculation screening
Neighbouring active site
d-band modulation

ABSTRACT

The high-performance electrocatalyst play an important role for hydrogen evolution reaction(HER) in water electrolysis. The tedious catalyst development experiment and precise design of catalytically active sites arouse researcher's great interest on the integrative research of theory and experiment. Herein, cobalt-based dual-atom catalysts were rationally screened according to density functional theory calculation firstly. Then, the potentially and highly active dual-atom catalysts Co-M DAC(M = Fe, Cu, Zn) were successfully prepared on carbon paper (CP). The prepared CoCu DAC@CP and CoFe DAC@CP exhibit excellent HER activity, markedly higher than the Co single atom catalyst under the respectively same experimental conditions. Further theoretical studies reveal that the superior activity can be attributed to neighbouring active site (Co, M and Co-M sites; M = Fe, Cu). The consistency between experiment and theoretical calculation demonstrates the orientation of future research prospective in DFT calculation assisted HER catalyst development.

1. Introduction

The use of hydrogen produced by water electrolysis can alleviate the pressure of traditional fossil energy shortage and environmental pollution. This provides a solution for sustainable energy since hydrogen is an ideal substitute for fossil fuels [1–4]. Hydrogen energy has received unprecedented attention worldwide. The hydrogen produced by water electrolysis with renewable electricity is regarded as carbon-neutral and sustainable, namely well-known green hydrogen. Nevertheless, the traditional Pt-based noble metals electrocatalysts are too expensive to be widely used for hydrogen evolution reaction (HER). Therefore, development of highly efficient and low-cost HER catalyst is an urgent need for promoting large-scale application of water electrolysis [5–14].

Single-atom catalysts (SAC) have become very popular in catalytic chemistry since they were firstly reported by Zhang et al. in 2011 [15]. The low-cost transition metal (Co, Mo, W, etc.) single-atom catalysts were reported for hydrogen production by water electrolysis and showed good activity [16–20]. For example, the active center Co atom of Co single-atom catalyst (Co-N_4/C) has a relatively proper adsorption of H in acidic condition, which is favorable to hydrogen evolution reaction [20]. However, the active sites are isolated single sites in typical SACs. Theoretically, two adjacent active sites are beneficial to the Heyrovsky reaction ($H^* + H_2O + e^- \rightarrow H_2 + OH^-$) or Tafel reaction ($H^* + H^* \rightarrow H_2$) according to hydrogen evolution mechanism. Single atoms catalyst with single active sites hardly meets this expectation [21].

Under this circumstance, dual-atom catalysts (DACs) have recently emerged as a further expansion to the family of SACs, which have the potential to meet above requirement of two adjacent active sites. Additionally, DACs can also adjust the d-band by the interaction of electronic orbits of dual metallic atoms and optimize the adsorption energy of intermediates [22,23]. A series of dual-atom catalysts have shown excellent activity for different reactions due to their unique structure [24–32]. However, to build an DAC catalyst with excellent HER activity is not easy. Besides the precise and controllable synthesis of DAC catalyst, the number of combined dual atoms in DAC would be numerous. A large number of experiments for catalyst screening and optimizing are necessary. Up to now, there are limited papers that reported active DAC catalyst for HER reaction [27,29,33,34], particularly for non-noble metal catalyst [29,34].

It is well known that the adsorption ability for H atom on the catalyst surface (ΔG_{H^*}) is an important descriptor to the catalytic activity of the HER catalyst [35–37]. An ideal HER catalyst should have a moderate

* Corresponding author at: Qingdao Institute of Bioenergy and Bioprocess Technology, Chinese Academy of Sciences, Qingdao 266101, Shandong, China.
E-mail address: liulc@qibebt.ac.cn (L. Liu).

https://doi.org/10.1016/j.apcatb.2022.122244
Received 23 August 2022; Received in revised form 26 November 2022; Accepted 29 November 2022
Available online 1 December 2022

ΔG_{H^*} value (close to 0 eV), such as − 0.09 eV of ΔG_{H^*} for Pt(111). Although it is not comprehensive to understand the HER activity of a catalyst from the adsorption energy of H merely, the hydrogen evolution performance of a catalyst could be generally predicted preliminary based on the adsorption energy of H, namely the closer $|\Delta G_{H^*}|$ value to 0 eV, the more active for hydrogen evolution [20].

On this consideration, quantum chemistry calculations were applied initially to assist catalyst screening for cobalt-based Co-M dual-atom DAC catalysts in this paper. A series of Co-M (M = Cu, V, W, Mo, Fe, Zn, Co) model DAC catalysts structure was constructed and the H adsorption ability on the Co-M catalysts was calculated. Afterward, potential hydrogen generation catalysts ($|\Delta G_{H^*}|$ value close to 0 eV) were selected purposely, including three typical Co-M dual-atom catalysts of CoCu, CoZn and CoFe DAC. These three DACs were prepared by a modified chemical vapor deposition method [27]. Electrochemical tests reveal that CoCu DAC and CoFe DAC exhibit excellent HER activity under acidic and alkaline electrolyte, respectively. Further characterizations and DFT calculations manifest that Co-M paired dual-atoms not only provide neighbouring active site, but also create more catalytic activity reaction sites than that of single Co atoms catalyst, thus promoting HER activity.

2. Experimental detail

2.1. Catalyst preparation

The Co SAC@CP was prepared by a modified electrochemical plating method [38]. HCl (8 mL) + water (87.5 mL) + aniline (4.5 mL) was used as electrolyte. Graphite rod and Ag/AgCl (in saturated KCl) were used as counter electrode and reference electrode, respectively. A cleaned carbon paper was used as working electrode and the electroplating area was 1 × 1 cm^2. The electroplating voltage was 1.0 V and the electroplating time was 10 min. After that, carbon paper was washed with water and dried at 60 ℃ in a vacuum oven. The slice was labeled as PANI@CP. Then, the PANI@CP was immersed into $CoCl_2$ solution (0.1 M) and placed for 4 h in room temperature. Subsequently, the slice was token out and dried. The dried slice was placed in a tubular furnace, and the temperature was raised to 750 ℃ in a rate of 2 ℃/min and kept at the temperature for 3 h in a Ar gas flow. After treatment with 1.0 M H_2SO_4 at room temperature for 24 h, the black slice was taken out, dried and labeled as Co SAC@CP.

For synthesizing CoCu DAC@CP, CoFe DAC@CP and CoZn DAC@CP, the above Co SAC@CP catalyst was put into a tubular furnace, with 0.4 mmol ferrous chloride($FeCl_2$), copper acetate monohydrate($Cu(CO_2CH_3)_2H_2O$), or zinc acetate($(CH_3COO)_2Zn$) at the upstream of the stream. Then the temperature was raised up to 700 ℃, 250 ℃, or 250 ℃, respectively, in a rate of 2 ℃/min and keep for 2 h. After that, the temperature was raised to 750 ℃ for 2 ℃/min and kept at 750 ℃ for 1 h. The obtained black slice was pickling in 5.0 M H_2SO_4 for 24 h at room temperature. After cleaning and drying, the obtained black slice was labeled as CoFe DAC@CP, CoCu DAC@CP, CoZn DAC@CP, respectively.

2.2. Characterizations

The X-ray diffraction (XRD) patterns were collected on D8 advance X-ray Diffractometer from Bruker (Cu Kα radiation, scan rate: 5°/min, scan range: 5°–80°). Hitachi S-4800 high-resolution electron microscope was used to record the scanning electron microscope (SEM) pictures. The high-resolution TEM (HRTEM) and the energy-dispersive spectroscopy (EDS) mapping were recorded on a JEOL JEM-ARF200F TEM/STEM. A PHI Quantera SXM spectrometer with a monochromator and Al anode target at 40 kV were used to take X-ray photoelectron spectroscopy (XPS). The referencing C 1 s peak at 284.8 eV was used to calibrate the binding energy. X-ray absorption fine structure spectra (XAFS) was collected at BL14W1 beamline of Beijing Synchrotron Radiation Facility (BSRF) with a fluorescence model. Co foil, Fe foil, Cu foil and Zn foil were used as standard reference sample. Athena and Artemis codes were used to analyze the data. XANES and Fourier-transformed EXAFS were used to analyze the coordination environment of metal sites.

2.3. Electrochemical measurements

HER activity were investigated under a standard three-electrode system with a potentiostat (CHI 660, Shanghai Chenhua Ltd. Co.). Ag/AgCl (in saturated KCl) and graphite rod were acted as the reference and counter electrode, respectively. The CoCu DAC@CP, CoZn DAC@CP, CoFe DAC@CP and Co SAC@CP were directly used as the working electrode (1.0 ×1.0 cm^2) with loading amount of ~0.27 mg/cm^2. The commercial 20 % Pt/C were loaded onto carbon paper (CP) with ~2.8 mg/cm^2. 6 mg of 20 % Pt/C were dispersed in a mixture isopropanol /5 % Nafion solution ($V_{isopropanol}$ = 350 μL, $V_{Nafion\ solution}$ = 70 μL) by sonication, to form a homogeneous ink, and then dropped onto CP.

HER polarization curves were recorded by Linear sweep voltammetry (LSV) in 0.5 M H_2SO_4 and 1.0 M KOH with 5 mV/s. The iR-correction was manually performed. Electrochemical impedance spectra (EIS) were measured from 10^{-2} to 10^6 Hz, with an amplitude of 5 mV. Double-layer capacitance (C_{dl}) cyclic voltammetry with different sweep rates in a nonfaradic potential range.

2.4. Computational details

All the calculations were performed within the Plane-wave density functional theory (DFT) calculations using the CASTEP code of the Materials Studio package of Accelrys Inc.Perdew-Burke-Ernzerhof (PBE) was employed to model the exchange correlation energy within the generalized-gradient approximation (GGA). Considering both the calculation efficiency and accuracy, cutoff energy was set as 380 eV. Gamma point centered k-point meshes used for Brillouin zone were 2 × 3 × 1. The convergence tolerances for geometry optimization calculations were set to the maximum displacement of 0.001 Å, the maximum force of 0.03 eV/Å, the maximum energy change of 1.0 × 10^{-5} eV/atom and the self-consistent field (SCF) convergence tolerance was set to 1.0 × 10^{-6} eV/atom. The hydrogen adsorption free energy ΔG_{H^*} is calculated by $\Delta G_{H^*} = E_{(surf+H)}-E_{(surf)}-1/2E_{(H2)}+ \Delta E_{ZPE}-T\Delta S+ \Delta G_{pH}$, where ΔE_{ZPE} and ΔS are the difference in the zero-point energy and entropy between the adsorbed H atom and the gaseous phase H_2. In this study, the value of Δ_{ZPE}-TΔS was approximated as 0.24 eV at T = 300 K[39]. The $\Delta G_{pH} = 2.303 \times k_BT \times$ pH (k_B is the boltzmann constant, 1.38 ×10^{-23} J/K) indicates the free energy determined by the concentration of H^+ in the environment. To simulate the effect of pH value in 0.5 M H_2SO_4, the pH value was set to 0; to simulate the effect of pH value in 1.0 M KOH, the pH value was set to 14.

The $FeCl_2$ adsorption free energy $\Delta E_{(FeCl2)} = E_{(surf+FeCl2)} - E_{(surf)} - E_{(FeCl2)}$; The $Cu(CO_2CH_3)_2$ adsorption free energy $\Delta E_{(Cu(CO2CH3)2)} = E_{(surf+Cu(CO2CH3)2)} - E_{(surf)} - E_{(Cu(CO2CH3)2)}$; The $Zn(CO_2CH_3)_2$ adsorption free energy $\Delta E(Zn(CO_2CH_3)_2) = E_{(surf+Zn(CO2CH3)2)} - E_{(surf)} - E_{(Zn(CO2CH3)2)}$; The H_2O adsorption free energy $\Delta E_{(H2O^*)} = E_{(surf+H2O)} - E_{(surf)} - E_{(H2O)}$; The OH adsorption free energy $\Delta E_{(OH^*)} = E_{(surf+OH)} - E_{(surf)} - E_{(OH)}$.

3. Results and discussion

3.1. Activity prediction by theoretical calculation

The typical Co-N_4/C SAC's structure is shown as Fig. 1a, Co atom is coordinated with four N atoms in the pyridine ring. And the typical Co-M dual-atoms (Fig. 1b) were built based on the previous report [25,28,30]. Density functional theory (DFT) method was used to calculate the Gibbs free energy for H adsorption (ΔG_{H^*}) on Co SAC and CoM DAC catalysts, which was used to predict the hydrogen evolution abilities (Fig. 1c, S1). Single atom Co SAC and dual atoms CoCo DAC were also calculated as comparison. The ΔG_{H^*} of Co SAC was calculated to be 0.10 eV, close to the value of previous report (0.13 eV) [20], implying that

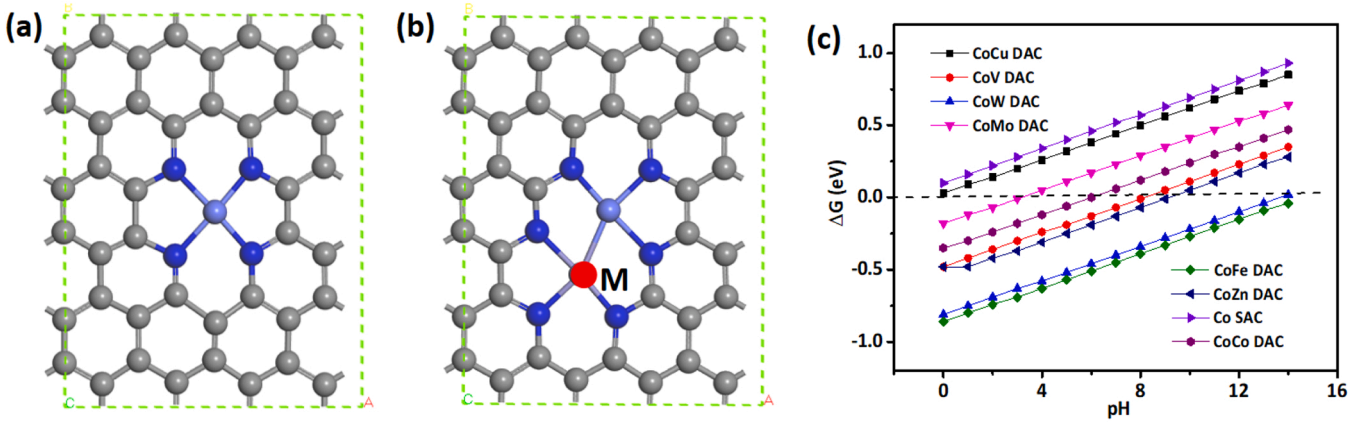

Fig. 1. Structure diagram of Co SAC (a) and CoM dual-atom catalysts (b), in which gray is C, dark blue is N, light blue is Co, white is H; M = Cu, V, W, Mo, Fe, Zn and Co. Gibbs free energy for H adsorption (ΔG_{H^*}) on single Co atoms catalyst and different CoM dual-atom catalysts (c).

the calculation results are repeatable and comparable. The calculated ΔG_{H^*} of CoCu DAC (0.03 eV), Co SAC (0.10 eV) and CoMo DAC (−0.18 eV) are all close to 0 eV ($|\Delta G_{H^*}| < 0.3$ eV) in acidic electrolyte (pH = 0), which indicates that these three catalysts have potential to give better HER activity than the others in acidic electrolyte. Differently, the ΔG_{H^*} of CoFe DAC (−0.04 eV) and CoW DAC (0.02 eV) were calculated to be closer to 0 eV than the others in alkaline electrolyte (pH = 14), implying that CoFe DAC and CoW DAC could perform better for hydrogen evolution under alkaline electrolyte. Therefore, CoCu DAC (performing better under acidic condition) and CoFe DAC (performing better under alkaline condition) were chosen to be prepared and investigated experimentally. Additionally, Co SAC and CoZn DAC were also synthesized as references.

3.2. Morphology and structure

The CoCu, CoFe and CoZn dual-atom catalysts were prepared on cleaned carbon papers (CP) via a simple chemical vapor deposition

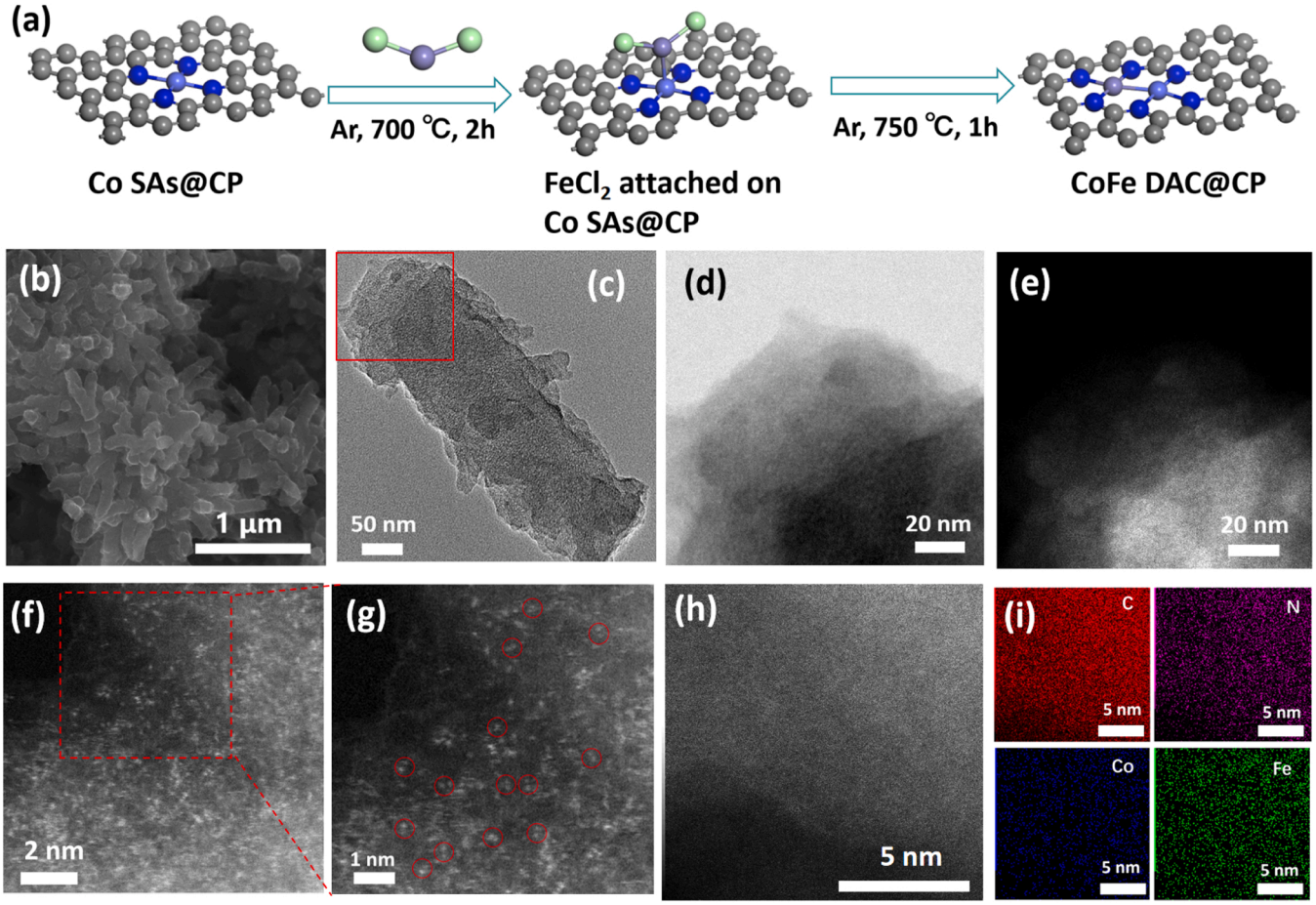

Fig. 2. Schematic illustration for the formation of CoFe DAC (a); SEM images of CoFe DAC (b); TEM images of CoFe DAC (c); a larger HAADF-STEM images of CoFe DAC (d, e) of the square area selected in (c); Aberration-corrected high-angle annular dark-field STEM (HAADF-STEM) image (f, g); HAADF-STEM image (h) and corresponding element distribution (i) with C, N, Co and Fe.

method from Co SAC@CP (Fig. 2a). Typically, the commercial bare carbon paper (CP) composed of interwoven carbon fibers was used as substrate (Fig. S2). The Co SAC@CP was firstly synthesized by a modified electrochemical plating method on bare CP [38]. Then, taking CoFe DAC@CP as an example, the Co SAC@CP was placed in a tube furnace with 0.4 mmol ferrous chloride hexahydrate ($FeCl_2{\cdot}6\,H_2O$) at the upstream of the airstream. The temperature was raised up to 700 ℃ and kept for 2 h in an Ar gas flow. In this process, ferrous chloride ($FeCl_2$) was gasified and attached on the Co site on Co SAC@CP since that the boiling point of ferrous chloride ($FeCl_2$) is close to 700 ℃ (Fig. 2a). Theoretically, the electron cloud of Fe atom would be more likely to interact with the electron cloud of Co atom. The calculated negative value of adsorption energy for $FeCl_2{\cdot}6\,H_2O$ on Co SAC@CP (Fig. S3a) suggests that the $FeCl_2$ molecule prefer to attach on the Co atom of Co SAC@CP. Then, the Fe atoms of $FeCl_2$ bonded to the Co atoms of Co SAC@CP and formed CoFe DAC@CP after high temperature treatment (750 ℃, 1 h) in Ar gas flow. Similar process could happen when the gasified molecules were copper acetate or zinc acetate (Fig. S3, b-c). Finally, the obtained black slice retains dual-atomic structure after pickling in 5.0 M H_2SO_4 for 24 h at room temperature.

SEM and TEM images of the CoFe DAC indicate that it's short rod-like shape on the carbon paper (Figs. 2b-c, S4) and no metal particles are observed in HRTEM images (Fig. 2d-e), implying the mono-dispersion of metal atoms. Aberration-corrected high-angle annular dark-field STEM (HAADF-STEM) image in Fig. 2f-g clearly demonstrates the existence of dual-atom pairs, as marked by several red cycles. Statistical analysis of dual atoms showed a Co-Fe distance of 0.22 nm (Fig. S5a). Lattice distortion defects characteristic (Fig. S5b-c) suggests the coordination of Co and Fe atoms with nitrogen. HAADF-STEM (Fig. 2h) and elemental mapping (Fig. 2i) reveal that C, N, Co and Fe are distributed evenly in CoFe DAC. Furthermore, the atomic pairs bonded by Co and Fe can be speculated in the dashed red box of an enlarged High resolution HAADF-STEM element mapping study (Fig. S6). The prepared CoCu DAC, CoZn DAC and Co SAC also show similar short rod-like structures without nanoparticles (Figs. S7-S10).

The CoCu, CoFe, CoZn DAC@CP and Co SAC@CP all exhibit two characteristic diffraction peaks in X-ray diffraction (XRD) patterns at about 26.5° and 54.6° (Fig. S11), which are ascribed to graphite (111) and (222) planes (PDF#75-2078). No metal or metal oxides diffraction peaks are observed. The Raman spectra (Fig. S12) show typical carbon peaks at about 1350 cm^{-1} (D band) and 1580 cm^{-1} (G band) for all the four catalysts. The ratio I_D/I_G of CoCu DAC@CP, CoFe DMC@CP and CoZn DMC@CP are 1.01, 0.98 and 0.96, respectively, indicating the intense carbon defects caused by metal and nitrogen doping. X-ray photoelectron spectroscopy (XPS) of CoCu, CoFe and CoZn DAC@CP shows $C_{1\,s}$, $N_{1\,s}$, $O_{1\,s}$, Co_{2p} and $Cu_{2p}/Fe_{2p}/Zn_{2p}$ peaks (Fig. S13). The C1s spectrum shows sp^2 C (284.8 eV), sp^3 C (285.7 eV) and C-O_x (286–288 eV)[26,28] (Fig. S14). The sp^2 C content of CoCu DAC@CP, CoFe DAC@CP and CoZn DAC@CP are all lower than that of Co SAC@CP because of the doping of heteroatoms (Table S1) [28]. The N 1 s spectrum of the four catalysts shows pyridinic N (398.4 eV), metal-N (399.7 eV), pyrrolic N (400.7 eV) and graphitic N (401.4 eV) (Fig. S15) [28]. Due to higher metal doping, there are less graphitic N and more Metal-N in the Co-M dual-atom catalysts of CoCu, CoFe and CoZn DAC@CP than that in the Co SAC@CP (Table S2). The 2p signals of Co/Cu/Fe/Zn imply positive valence state of those metals (Fig. S16), indicates the existence of Metal-N [26,30,39–41].

X-ray absorption near-edge structure (XANES) and extended X ray absorption fine structure measurements (EXAFS) were conducted to explore the electronic structure and the coordination environment of metal atoms. The absorption edge of Co Kedge for CoCu, CoFe, CoZn DAC@CP and Co SAC@CP are all shifted ~3.0 eV towards lower energy

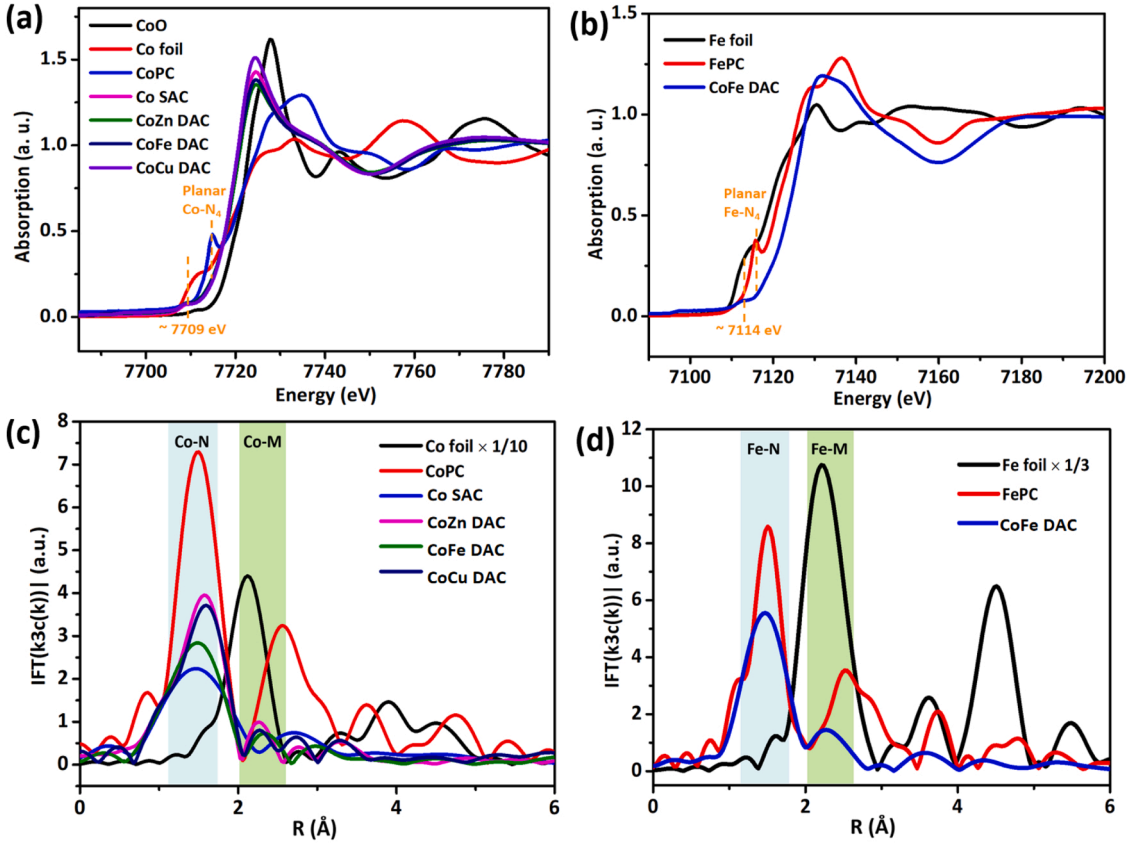

Fig. 3. Co K-edge XANES (a) and Fourier-transform EXAFS spectra (c) of different samples; Fe K-edge XANES (b) and Fourier-transform EXAFS spectra (d) of different samples.

relative to CoO, indicating that the valence state of Co for the Co-M dual-atoms is situated between that of Co^{0+} and Co^{2+} (Fig. 3a) [28]. The pre-edge peak at ~7709 eV in Co K-edge XANES of the four samples indicates a 1 s to 4pz shakedown transition of a square-planar coordination with $D_{4\,h}$ local symmetry [42]. This implies that the presence of Co coordinated with four nearest atoms (nitrogen or metal) in dual-atomic coordination. The absorption edge of Fe Kedge of CoFe DAC@CP was similar to that of FePC and between those of FePC and Fe foil (Fig. 3b), indicating that the valence state of Fe is situated between that of Fe^{0+} and Fe^{2+}[43,44]. Pre-edges recorded at ~7114 eV for CoFe DAC in the Fe K-edge XANES (Fig. 3b) manifest the formation of X-ray absorbing Fe centers combined with four neighbor atoms [42,45–48]. The observed positive valence states for Co and Fe, instead of metallic states, further affirming their isolated coordination configurations [28,48]. In Co EXAFS spectra of the Co-M dual-atom catalysts (Fig. 3c), the peaks at ~1.50 Å and ~2.30 Å are ascribed to the Co-N [20,25,49] and Co-M/Co-C [25,26,48] coordination, respectively. EXAFS fitting results (Fig. S13 and Table S4) confirms dual-atomic local structure in CoFe DAC, CoCu DAC and CoZn DAC. Similarly, the main peak at 1.47 Å and 2.27 Å in Fe EXAFS spectra of CoFe DAC (Fig. 3d) are ascribed to Fe-N coordination [30,45,48] and Fe-M/Fe-C coordination [41,50] in EXAFS fitting (Fig. S17), indicating the dual-atomic local structure in CoFe DAC. The Cu EXAFS spectra and Zn EXAFS spectra also imply the same dual-atomic structure in CoCu DAC and CoZn DAC (Fig. S17 and Table S4) [41,51,52]. The detailed fitting results can be found in the Supporting Information (Fig. S17 and Table S4). The bond length of M-N and M-M of FT EXAFS for Co-M dual-atom are close to the data of simulation model (Table S5).

3.3. Hydrogen evolution reaction performance of Co-M dual-atom catalysts

According to above prediction by DFT calculations (Section 3.1), the Co-M dual-atom catalysts could show outstanding catalytic activity for hydrogen evolution under different pH values of electrolyte. Then, the hydrogen evolution reaction performance of prepared DAC catalysts was investigated in 0.5 M H_2SO_4 or 1.0 M KOH electrolyte by using a standard three-electrode setup. Based on the reference electrode calibration (Fig. S18), the measured potentials (vs. Ag/AgCl) were converted to the reversible hydrogen electrode (RHE). The commercial 20 % Pt/C, Co SAC@CP and bare carbon paper (CP) were also tested as a comparison. From Fig. 4a-d, the CoCu DAC@CP appears high HER activity under 0.5 M H_2SO_4 compared with other catalysts. The CoCu DAC@CP produces cathodic geometric current density (j) of 20 mA cm^{-2} at an overpotential of 90 mV (η_{20} = 90 mV), much lower than those of Co SAC@CP (148 mV), CoZn DAC@CP (194 mV), CoFe DAC@CP (220 mV) and bare CP (>800 mV) (Fig. 4a, c). Interestingly, activity sequence is following the DFT prediction results exactly. Moreover, CoCu DAC@CP affords a small Tafel slope of 92.4 mV/dec, which is also much lower than those of Co SAC@CP (136.7 mV/dec), CoZn DAC@CP (107.2 mV/dec), CoFe DAC@CP (127.1 mV/dec) and bare CP (366.6 mV/dec) (Fig. 4b), reflecting that CoCu DAC@CP has relatively higher HER kinetic process under acid conditions. The Tafel slope of Co SAC@CP (136.7 mV/dec) suggests a Volmer mechanism. While, the lower Tafel slope of CoCu DAC@CP (92.4 mV/dec) suggests a Volmer-Heyrovsky mechanism [21]. This indicates that the CoCu DAC@CP could promote the Heyrovsky reaction ($H^* + H_3O^+ + e^- \rightarrow H_2 + H_2O$) of hydrogen evolution. Turnover frequency (TOF) of different catalyst in 0.5 M H_2SO_4 (Fig. S19a) indicates the excellent intrinsic activity of CoCu DAC@CP with remarkable TOF value of 1.23 s^{-1} at 200 mV. The potentiostatic test indicates CoCu DAC@CP can maintain a constant HER current density (~25 mA cm^{-2}) in 0.5 M H_2SO_4 even after 60 h (Fig. 4d). Moreover, the LSV curve of CoCu DAC@CP also shows a slight difference after 5000 CV cycles, suggesting its long-term stability for acidic HER (inset Fig. 4d).

In comparison, the CoFe DAC@CP shows higher HER activity in 1.0 M KOH than others (Fig. 4e-h). The CoFe DAC@CP produces cathodic geometric current density (j) of 20 mA cm^{-2} at a low overpotential of 21.5 mV (η_{20} = 21.5 mV). A small Tafel slope of 62.9 mV/dec for CoFe DAC@CP manifests higher HER kinetic process than the others. Furthermore, the lower Tafel slope of CoFe DAC@CP (62.9 mV/dec) suggests a Volmer-Heyrovsky mechanism [21]. While the Tafel slope of Co SAC@CP (136.9 mV/dec) suggests a Volmer mechanism. This indicates that the CoFe DAC@CP may promote the Heyrovsky reaction ($H^* + H_2O + e^- \rightarrow H_2 + OH^-$) of hydrogen evolution, meeting our expectation. The calculated turnover frequency (TOF) is 1.63 s^{-1} at 200 mV in 1.0 M KOH (Fig. S19b), indicates the excellent intrinsic activity of CoFe DAC@CP. Long life test of 60 h indicates that CoFe DAC@CP can maintain a constant HER current density at ~20 mA cm^{-2} (Fig. 4h). The LSV curve of CoFe DAC@CP also shows a negligible difference after 5000 CV cycles, suggesting its long-term stability for alkaline HER (inset of Fig. 4h).

The corresponding Nyquist plots further indicate that CoCu DAC@CP possesses much smaller electrochemical impedance than Co SAC@CP, CoZn DAC@CP, CoFe DAC@CP and bare CP (Fig. S20a) in 0.5 M H_2SO_4, indicate faster charge-transfer capacity of CoCu DAC@CP than others during hydrogen evolution. Similarly, CoFe DAC@CP possesses much smaller electrochemical impedance than other catalysts in 1.0 M KOH (Fig. S20b). This implies that different electrolyte environment has great impact on different Co-M catalysts. The C_{dl} (double-layer capacitance) of CoCu DAC@CP is 547.1 mF cm^{-2}, much higher than that of other catalysts (Fig. S21), indicating a significant enhanced electrochemical active surface area (ECSA). Due to the dual-atomic structure, the C_{dl} of CoCu DAC@CP, CoFe DAC@CP and CoZn DAC@CP are all higher than that of Co SAC@CP (185.9 mF cm^{-2}). This implies that the Co-M dual-atom could provide more effective electrochemical surface. Furthermore, geometric current density was normalized by electrochemical active surface area (ECSA; j_{ECSA}) based on the calculated C_{dl} (Fig. S22). The result indicates that the high intrinsic activity of CoCu DAC@CP. Furthermore, the Faradic efficiency was calculated by measuring the amount of H_2 at a constant current (~ 200 mA cm^{-2}) at different time (Fig. S23) for both CoCu DAC@CP in 0.5 M H_2SO_4 and CoFe DAC@CP in 1.0 M KOH, the result suggesting almost 100 % Faradic efficiency. The XRD and XPS after HER test for the prepared Co-M dual-atom catalyst show no apparent difference with the fresh one (Figs. S24 and S25). Additionally, the HR-TEM of the Co-M dual-atom catalyst shows no accumulation of metal particles (Fig. S26). All this indicates the strong stability of the catalysts.

Overall, the prepared Co-M dual-atom catalyst exhibit competitive hydrogen evolution activity with other reported non-noble metals single atoms and dual-atom catalysts for hydrogen evolution with low metal loading (Tables S6 and S7). CoCu DAC@CP shows excellent catalytic activity under acidic conditions, in contrast, CoFe DAC@CP shows the highest catalytic activity under alkaline conditions. More Co-M dual-atom catalysts will be prepared and a deep research will be taken in the future. The experimental results basically accord with the expectation of DFT calculation prediction. However, the wide applicability and intrinsic mechanism for this phenomenon still needs in-depth studies.

3.4. The origin of high efficiency for hydrogen evolution reaction on Co-M DACs

DFT method was also used for the investigation the origin of the different hydrogen evolution activity for different catalysts (Figs. 5 and S27). The above hydrogen evolution reaction performance suggests a Volmer-Heyrovsky mechanism for both CoCu DAC@CP under acidic conditions and CoFe DAC@CP under alkaline conditions based on the lower Tafel slope[21]. Therefore, Volmer-Heyrovsky mechanism was simulated firstly.

For the hydrogen evolution on CoCu DAC under acidic condition (simulated environment: pH = 0; red line in Fig. 5a), the catalyst active site receives a hydrated proton H_3O^+ and an electron, to form a structure

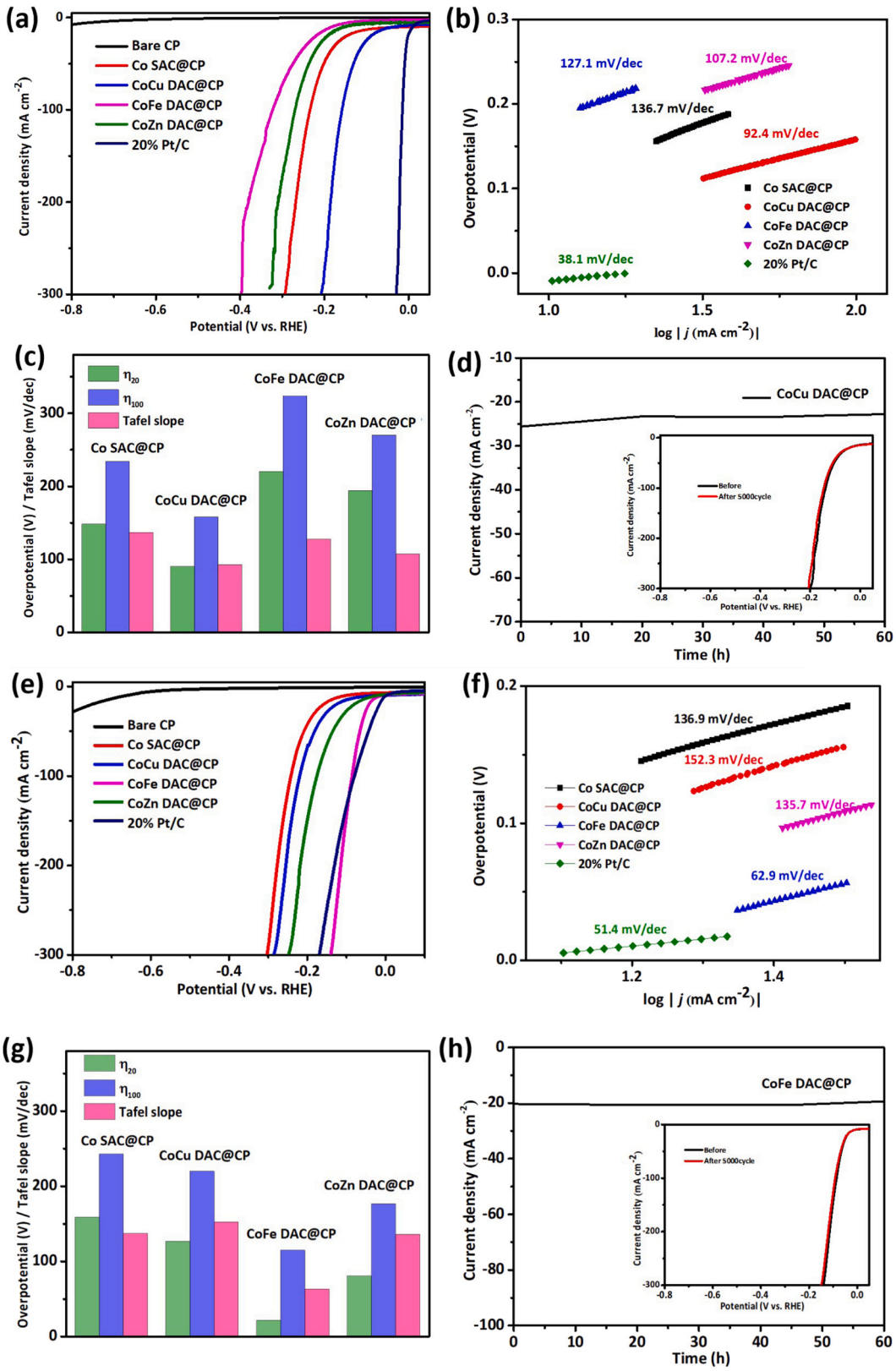

Fig. 4. HER activity evaluation in 0.5 M H_2SO_4 (a-d) and 1.0 M KOH (e-h). The polarization curves (a, e) and the corresponding Tafel plots (b, f) of different catalysts; comparison of different catalysts in 0.5 M H_2SO_4 (c) and 1.0 M KOH (g); Constant potentials test recorded on CoCu DAC@CP at a cathodic current density of ~25 mA cm^{-2} in 0.5 M H_2SO_4 (100 mV) with Polarization curves recorded from CoCu DAC@CP catalyst before and after 5000 potential cycles between − 0.15 V and − 0.30 V (vs Ag/AgCl) in 0.5 M H_2SO_4 inset (d); Constant potentials test recorded on CoFe DAC@CP at a cathodic current density of ~20 mA cm^{-2} in 1.0 M KOH (30 mV)with polarization curves recorded from CoFe DAC@CP catalyst before and after 5000 potential cycles between − 0.95 V and − 1.10 V (vs Ag/AgCl) in inset (h).

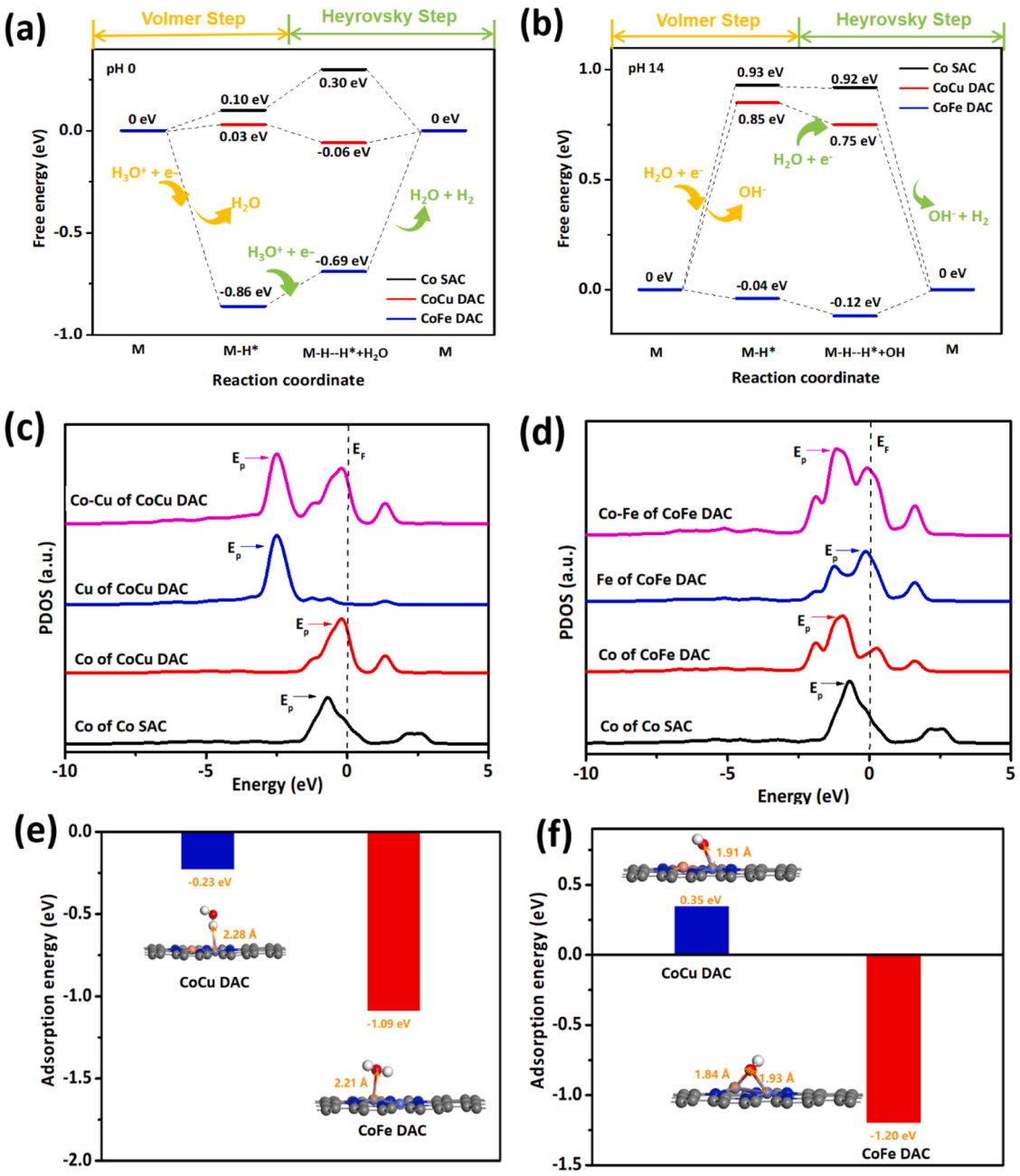

Fig. 5. Free energy diagram of CoCu DAC, CoFe DAC and Co SAC under acidic (a) and alkaline (b) conditions, the "**M**" here represent the CoCu DAC, CoFe DAC and Co SAC, respectively. Calculated partial densities of states (DOS) of d orbits for CoCu DAC, CoFe DAC and Co SAC with the Fermi level aligned at 0 eV (c and d); Calculated absorption energies of H_2O (e) and OH (f) on CoCu DAC and CoFe DAC with corresponding optimized structures insert.

with H adsorbed on the surface of the catalyst (**CoCu DAC-H***, relative energy is 0.03 eV), and then release a H_2O molecule. Then, **CoCu DAC-H*** combines with another H_3O^+ and another electron to get **CoCu DAC-H–H*** $+\mathbf{H_2O}$ (relative energy −0.06 eV). After that, the **CoCu DAC-H–H*** $+\mathbf{H_2O}$ releases a $\mathbf{H_2O}$ and $\mathbf{H_2}$ molecule. The relative free energy of the two intermediates in the whole reaction pathway are both close to 0 eV, indicating that the CoCu DAC could have excellent activity for hydrogen evolution under acidic condition. For Co SAC and CoFe DAC (black line and blue line in Fig. 5a), the reaction pathways are similar to that of CoCu DAC under acidic conditions. The relative free energies of **CoFe DAC-H*** and **CoFe DAC-H–H*** $+\mathbf{H_2O}$ are − 0.86 eV and − 0.69 eV, respectively. The relative free energies of **Co SAC-H*** and **Co SAC-H–H*** $+\mathbf{H_2O}$ are 0.10 eV and 0.30 eV, respectively. These results indicate that CoFe DAC and Co SAC may not show excellent activity for hydrogen evolution under acidic conditions when comparing with that of CoCu DAC. Besides, the CoCu DAC could promote the Heyrovsky reaction ($H^* + H_3O^+ + e^- \rightarrow H_2 + H_2O$) of hydrogen evolution than the Co SAC, in consistent with our expectation and the hydrogen evolution reaction performance.

When the catalyst CoCu DAC was used under alkaline conditions (simulated environment: pH = 14; red line in Fig. 5b), CoCu DAC firstly combines with a H_2O molecule and an electron to obtain **CoCu DAC-H*** (0.85 eV) and release an OH^-. Then, the **CoCu DAC-H*** continues to adsorb another H_2O and electron and **CoCu DAC-H*** $+\mathbf{H_2O}$ is obtained. After that, the **CoCu DAC-H–H*** $+$**OH** releases another OH^- and H_2 molecule. The energy of **CoCu DAC-H–H*** $+$**OH** is 0.75 eV, indicates that it is relatively difficult for the hydrogen generation. For Co SAC and CoFe DAC, the reaction pathways are similar to that of CoCu DAC under

alkaline conditions (black line and blue line in Fig. 5b). The relative free energies of **Co SAC-H*** and **Co SAC-H–H*+OH** are 0.93 eV and 0.92 eV, respectively, under alkaline conditions. While the relative energies of **CoFe DAC-H*** and **CoFe DAC-H–H*+OH** under alkaline conditions are − 0.04 eV and − 0.12 eV, respectively, implies that the hydrogen evolution is more likely to occur under alkaline conditions catalyzed by CoFe DAC. DFT calculation results account for the experimental results satisfactorily. More importantly, the CoFe DAC reduced the relative free energy of the Heyrovsky step intermediate significantly, indicating that the CoFe DAC could promote the Heyrovsky reaction ($H^* + H_2O + e^- \rightarrow H_2 + OH^-$) of hydrogen evolution than that of Co SAC.

Besides, the Volmer-Tafel mechanism was also simulated and the details are shown in the Fig. S27. The data shows that the Tafel reaction is promoted for CoCu DAC under acidic conditions, while the Tafel reaction is promoted for CoFe DAC under alkaline conditions. Considering that the reaction is more likely follow the Volmer-Heyrovsky mechanism under the experimental conditions of this study. The update of experimental conditions and catalyst will be further studied to promote the Tafel reaction. All the calculation results indicate that Co-M dual-atom could provide neighbouring active site (Co sites, M sites and Co-M sites; M = Fe or Cu) for hydrogen evolution, which has obvious advantages than that of Co SAC (single active site). The neighbouring active sites promote the absorption of hydrogen atoms (especially the second H atom) by reducing the relative free energy significantly when compared with Co SAC, and thus improve the evolution of hydrogen.

Based on the previous report, the DOS peak is closer to the Fermi level and a stronger H* adsorption can be obtained[53]. The calculated partial density of state (PDOS) in Fig. 5c shows that the Co sites of CoCu DAC can promote H* adsorption because that the peak of d orbital of densities of states for Co sites is the closest to the Fermi level. This also indicates that Co sites of CoCu DAC are the most important active sites than Cu sites and Co-Cu bridge sites for hydrogen evolution for creates an opportunity for the Heyrovsky or Tafel reaction by promoting multiple H adsorption. Similarly, the peak of d orbital of densities of states for Fe sites is the closest to the Fermi level (Fig. 5d), indicates that the Fe sites of CoFe DAC are the most crucial active sites than Co sites and Co-Fe sites also by creates opportunity for the Heyrovsky or Tafel reaction by promote multiple H adsorption. In addition, both the peak of d orbital of densities of states for Co sites of CoCu DAC and Fe sites of CoFe DAC are more close to the Fermi level than the Co sites of Co SAC, which indicates that CoCu DAC and CoFe DAC could have a stronger H* adsorption than that of Co SAC. All this manifest that the Co-M dual-atom not only provides neighbouring active site (Co sites, M sites and Co-M sites; M = Fe or Cu), but also creates more crucial activity sites (Co sites of CoCu DAC and Fe sites of CoFe DAC) than Co single atom catalysts (Co sites) for hydrogen evolution.

Further study of the adsorption for H_2O on CoCu DAC and CoFe DAC (Fig. 5e) indicates that the H atom of H_2O prone to attached on the Co atom of CoCu DAC, while the O atom of H_2O easily absorbed on the Fe atom of CoFe DAC. Moreover, the OH are more easily to be adsorbed on CoFe DAC provided by a relative negative energy than that on CoCu DAC (Fig. 5f). This indicates that CoFe DAC could grab OH easily and thus create an opportunity for promoting the hydrogen evolution under a reaction system with plentiful OH (alkaline conditions). We believe that each catalysts or each active sites have its suitable reaction environments for for the catalytic reaction. We encourage that the catalytic environments also been taken more consideration.

4. Conclusions

Co-M dual-atom catalysts were firstly pre-screened based on DFT calculations. Accordingly, the potentially active Co-M dual-atom catalysts, including CoCu DAC@CP, CoFe DAC@CP and CoZn DAC@CP, were prepared by a simple chemical vapor deposition method. The as-prepared CoCu DAC@CP and CoFe DAC@CP showed complete dual atomic structure and achieved excellent HER activity under acidic and alkaline conditions, respectively, which was perfectly consistent with the DFT calculation prediction. Depth study indicates that OH are more easily to be adsorbed on CoFe DAC, leading to a promoted hydrogen evolution under alkaline conditions. The proper Co-M dual-atom catalysts provide neighbouring active site and promote the Heyrovsky reaction of hydrogen evolution than that of the Co SAC, completely meet our expectations. Furthermore, the Co-M DAC exhibits more active hydrogen evolution reaction sites than Co SAC by adjusting the peak of d-band, thus promoting the hydrogen evolution reaction.

CRediT authorship contribution statement

Mingyang Jiao: Conceptualization, Methodology, Investigation, Funding acquisition, Writing. **Zhipeng Chen:** Formal analysis, Validation. **Nailiang Wang:** Formal analysis, Validation. **Licheng Liu:** Funding acquisition, Writing - editing.

Declaration of Competing Interest

The authors declare that they have no known competing financial interests or personal relationships that could have appeared to influence the work reported in this paper.

Data availability

Data will be made available on request.

Acknowledgements

The financial supports by Shandong provincial Natural Science Foundation (grant no. ZR2021QB157), National Natural Science Foundation of China (grant no. U21B2099). We acknowledge National Supercomputing Center in Shenzhen for providing the computational resources and materials studio (materials studio 7.0, CASTEP and Visualizer).

Appendix A. Supporting information

Supplementary data associated with this article can be found in the online version at doi:10.1016/j.apcatb.2022.122244.

References

[1] X. Zou, Y. Zhang, Noble metal-free hydrogen evolution catalysts for water splitting, Chem. Soc. Rev. 44 (2015) 5148–5180, https://doi.org/10.1039/C4CS00448E.
[2] J. Gu, J.A. Aguiar, S. Ferrere, K.X. Steirer, Y. Yan, C.X. Xiao, J.L. Young, M. Aljassim, N.R. Neale, J.A. Turner, A graded catalytic-protective layer for an efficient and stable water-splitting photocathode, Nat. Energy 2 (2017) 16192, https://doi.org/10.1038/nenergy.2016.192.
[3] C. Zhang, Y. Shi, Y. Yu, Y. Du, B. Zhang, Engineering sulfur defects, atomic thickness, and porous structures into cobalt sulfide nanosheets for efficient electrocatalytic alkaline hydrogen evolution, ACS Catal. 8 (2018) 8077–8083, https://doi.org/10.1021/acscatal.8b02056.
[4] Y. Pan, K. Sun, S. Liu, X. Cao, K. Wu, W.-C. Cheong, Z. Chen, Y. Wang, Y. Li, Y. Liu, D. Wang, Q. Peng, C. Chen, Y. Li, Core-shell ZIF-8@ZIF-67-derived CoP nanoparticle-embedded N-doped carbon nanotube hollow polyhedron for efficient overall water splitting, J. Am. Chem. Soc. 140 (2018) 2610–2618, https://doi.org/10.1021/jacs.7b12420.
[5] E. Hu, Y. Feng, J. Nai, D. Zhao, Y. Hu, X.W. (David) Lou, Construction of hierarchical Ni-Co-P hollow nanobricks with oriented nanosheets for efficient overall water splitting, Energy Environ. Sci. 11 (2018) 872, https://doi.org/10.1039/c8ee00076j.
[6] J. Chen, J. Liu, J.-Q. Xie, H. Ye, X.-Z. Fu, R. Sun, C.-P. Wong, Co-Fe-P nanotubes electrocatalysts derived from metal-organic frameworks for efficient hydrogen evolution reaction under wide pH range, Nano Energy 56 (2019) 225–233, https://doi.org/10.1016/j.nanoen.2018.11.051.
[7] X. Jia, Y. Zhao, G. Chen, L. Shang, R. Shi, X. Kang, G.I.N. Waterhouse, L.-Z. Wu, C.-H. Tung, T. Zhang, Ni_3FeN nanoparticles derived from ultrathin NiFe-layered double hydroxide nanosheets: an efficient overall water splitting electrocatalyst, Adv. Energy Mater. 6 (2016), 1502585, https://doi.org/10.1002/aenm.201502585.
[8] H. Fan, H. Yu, Y. Zhang, Y. Zheng, Z. Dai, B. Li, Y. Zong, Q. Yan, Fe-doped Ni_3C nanodots in N-doped carbon nanosheets for efficient hydrogen-evolution and

oxygen-evolution electrocatalysis, Angew. Chem. Int. Ed. 56 (2017) 12566–12570, https://doi.org/10.1002/anie.201706610.
[9] X. Liu, J. He, S. Zhao, Y. Liu, Z. Zhao, J. Luo, G. Hu, X. Sun, Y. Ding, Self-powered H_2 production with bifunctional hydrazine as sole consumable, Nat. Commun. 9 (2018) 4365, https://doi.org/10.1038/s41467-018-06815-9.
[10] Y. Yang, K. Zhang, H. Lin, X. Li, H.C. Chan, L. Yang, Q. Gao, MoS_2-Ni_3S_2 heteronanorods as efficient and stable bifunctional electrocatalysts for overall water splitting, ACS Catal. 7 (2017) 2357–2366, https://doi.org/10.1021/acscatal.6b03192.
[11] P. Wei, X. Li, Z. He, Z. Li, X. Zhang, X. Sun, Q. Li, H. Yang, J. Han, Y. Huang, Electron density modulation of MoP by rare earth metal as highly efficient electrocatalysts for pH-universal hydrogen evolution reaction, Appl. Catal. B Environ. 299 (2021), 120657, https://doi.org/10.1016/j.apcatb.2021.120657.
[12] Z. Xiao, M. Yang, J. Wang, Z. Xu, S. Zhang, A. Tang, R. Gao, H. Yang, FeNiP/MoOx integrated electrode grown on monocrystalline NiMoO4 nanorods with multi-interface for accelerating alkaline hydrogen evolution reaction, Appl. Catal. B Environ. 303 (2022), 120913, https://doi.org/10.1016/j.apcatb.2021.120913.
[13] W. Liu, X. Wang, J. Qu, X. Liu, Z. Zhang, Y. Guo, H. Yin, D. Wang, Tuning Ni dopant concentration to enable co-deposited superhydrophilic self-standing Mo2C electrode for high-efficient hydrogen evolution reaction, Appl. Catal. B Environ. 307 (2022), 121201, https://doi.org/10.1016/j.apcatb.2022.121201.
[14] D. Xiao, D.-L. Bao, X. Liang, Y. Wang, J. Shen, C. Cheng, P.K. Chu, Experimental and theoretical investigation of the control and balance of active sites on oxygen plasma-functionalized MoSe2 nanosheets for efficient hydrogen evolution reaction, Appl. Catal. B Environ. 288 (2021), 119983, https://doi.org/10.1016/j.apcatb.2021.119983.
[15] B.T. Qiao, A.Q. Wang, X.F. Yang, L.F. Allard, Z. Jiang, Y.T. Cui, J.Y. Liu, J. Li, T. Zhang, Single-atom catalysis of CO oxidation using Pt_1/FeO_x, Nat. Chem. 3 (2011) 634, https://doi.org/10.1038/NCHEM.1095.
[16] L. Cao, Q. Luo, W. Liu, Y. Lin, X. Liu, Y. Cao, W. Zhang, Y. Wu, J. Yang, T. Yao, S. Wei, Identification of single-atom active sites in carbon-based cobalt catalysts during electrocatalytic hydrogen evolution, Nat. Catal. 2 (2019) 134–141, https://doi.org/10.1038/s41929-018-0203-5.
[17] J.-D. Yi, R. Xu, G.-L. Chai, T. Zhang, K. Zang, B. Nan, H. Lin, Y.-L. Liang, J. Lv, J. Luo, R. Si, Y.-B. Huang, R. Cao, Cobalt single-atoms anchored on porphyrinic triazine-based frameworks as bifunctional electrocatalysts for oxygen reduction and hydrogen evolution reactions, J. Mater. Chem. A 7 (2019) 1252–1259, https://doi.org/10.1039/c8ta09490j.
[18] W. Chen, J. Pei, C. He, J. Wan, H. Ren, Y. Zhu, Y. Wang, J. Dong, S. Tian, W.-C. Cheong, S. Lu, L. Zheng, X. Zheng, W. Yan, Z. Zhuang, C. Chen, Q. Peng, D. Wang, Y. Li, Rational design of single molybdenum atoms anchored on N-doped carbon for effective hydrogen evolution reaction, Angew. Chem. Int. Ed. 56 (2017) 16086–16090, https://doi.org/10.1002/anie.201710599.
[19] W. Chen, J. Pei, C.-T. He, J. Wan, H. Ren, Y. Wang, J. Dong, K. Wu, W.-C. Cheong, J. Mao, X. Zheng, W. Yan, Z. Zhuang, C. Chen, Q. Peng, D. Wang, Y. Li, Single tungsten atoms supported on MOF-derived N-doped carbon for robust rlectrochemical hydrogen evolution, Adv. Mater. 30 (2018), 1800396, https://doi.org/10.1002/adma.201800396.
[20] M.D. Hossain, Z. Liu, M. Zhuang, X. Yan, G.-L. Xu, C.A. Gadre, A. Tyagi, I.H. Abidi, C.-J. Sun, H. Wong, A. Guda, Y. Hao, X. Pan, K. Amine, Z. Luo, Rational design of graphene-supported single atom catalysts for hydrogen evolution reaction, Adv. Energy Mater. 9 (2019), 1803689, https://doi.org/10.1002/aenm.201803689.
[21] S. Sultan, J.N. Tiwari, A.N. Singh, S. Zhumagali, M. Ha, C.W. Myung, P. Thangavel, K.S. Kim, Single atoms and clusters based nanomaterials for hydrogen evolution, oxygen evolution reactions, and full water splitting, Adv. Energy Mater. 9 (2019), 1900624, https://doi.org/10.1002/aenm.201900624.
[22] W. Zhang, Y. Chao, W. Zhang, J. Zhou, F. Lv, K. Wang, F. Lin, H. Luo, J. Li, M. Tong, E. Wang, S. Guo, Emerging dual-atomic-site catalysts for efficient energy catalysis, Adv. Mater. 33 (2021), 2102576, https://doi.org/10.1002/adma.202102576.
[23] J. Zhang, Q. Huang, J. Wang, J. Wang, J. Zhang, Y. Zhao, Supported dual-atom catalysts: preparation, characterization, and potential applications, Chin. J. Catal. 41 (2020) 783–798, https://doi.org/10.1016/S1872-2067(20)63536-7.
[24] Y. Li, Q. Zhang, C. Li, H.-N. Fan, W.-B. Luo, H.-K. Liu, S.-X. Dou, Atomically dispersed metal dimer species with selective catalytic activity for nitrogen electrochemical reduction, J. Mater. Chem. A 7 (2019) 22242, https://doi.org/10.1039/C9TA07845B.
[25] X. Han, X. Ling, D. Yu, D. Xie, L. Li, S. Peng, C. Zhong, N. Zhao, Y. Deng, W. Hu, Atomically dispersed binary Co-Ni sites in nitrogen-doped hollow carbon nanocubes for reversible oxygen reduction and evolution, Adv. Mater. 31 (2019), 1905622, https://doi.org/10.1002/adma.201905622.
[26] W. Zhu, L. Zhang, S. Liu, A. Li, X. Yuan, C. Hu, G. Zhang, W. Deng, K. Zang, J. Luo, Y. Zhu, M. Gu, Z.-J. Zhao, J. Gong, Enhanced CO_2 electroreduction on neighboring Zn/Co monomers by electronic effect, Angew. Chem. Int. Ed. 59 (2020) 12664–12668, https://doi.org/10.1002/anie.201916218.
[27] L. Zhang, R. Si, H. Liu, N. Chen, Q. Wang, K. Adair, Z. Wang, J. Chen, Z. Song, J. Li, M.N. Banis, R. Li, T.-K. Sham, M. Gu, L.-M. Liu, G.A. Botton, X. Sun, Atomic layer deposited Pt-Ru dual-metal dimer and identifying their active sites for hydrogen evolution reaction, Nat. Commun. 10 (2019) 4936, https://doi.org/10.1038/s41467-019-12887-y.
[28] Z. Lu, B. Wang, Y. Hu, W. Liu, Y. Zhao, R. Yang, Z. Li, J. Luo, B. Chi, Z. Jiang, M. Li, S. Mu, S. Liao, J. Zhang, X. Sun, An isolated zinc-cobalt atomic pair for highly active and durable oxygen reduction, Angew. Chem. Int. Ed. 58 (2019) 2622–2626, https://doi.org/10.1002/ange.201810175.
[29] Y. Yang, Y. Qian, H. Li, Z. Zhang, Y. Mu, D. Do, B. Zhou, J. Dong, W. Yan, Y. Qin, L. Fang, R. Feng, J. Zhou, P. Zhang, J. Dong, G. Yu, Y. Liu, X. Zhang, X. Fan, O-coordinated W-Mo dual-atom catalyst for pH-universal electrocatalytic hydrogen evolution, Sci. Adv. 6 (2020) eaba6586, https://doi.org/10.1126/sciadv.aba6586.
[30] X. Zhu, D. Zhang, C.-J. Chen, Q. Zhang, R.-S. Liu, Z. Xia, L. Dai, R. Amal, X. Lu, Harnessing interplay of Fe-Ni atom pairs embedded in nitrogen-doped carbon for bifunctional oxygen electrocatalysis, Nano Energy 71 (2020), 104597, https://doi.org/10.1016/j.nanoen.2020.104597.
[31] Y. Lia, C. Chen, R. Cao, Z. Pan, H. He, K. Zhou, Dual-atom Ag_2/graphene catalyst for efficient electroreduction of CO_2 to CO, Appl. Catal. B Environ. 268 (2020), 118747, https://doi.org/10.1016/j.apcatb.2020.118747.
[32] F. Kong, R. Si, N. Chen, Q. Wang, J. Li, G. Yin, M. Gu, J. Wang, L.-M. Liu, X. Sun, Origin of hetero-nuclear Au-Co dual atoms for efficient acidic oxygen reduction, Appl. Catal. B Environ. 301 (2022), 120782, https://doi.org/10.1016/j.apcatb.2021.120782.
[33] X. Yao, L. Zhang, Y. Jia, H. Liu, L. Zhuang, X. Yan, C. Lang, X. Wang, D. Yang, K. Huang, S. Feng, Charge polarization from atomic metals on adjacent graphitic layers for enhancing hydrogen evolution reaction, Angew. Chem. Int. Ed. 58 (2019) 9404–9408, https://doi.org/10.1002/ange.201902107.
[34] A. Kumar, V.Q. Bui, J. Lee, L. Wang, A.R. Jadhav, X. Liu, X. Shao, Y. Liu, J. Yu, Y. Hwang, H.T.D. Bui, S. Ajmal, M.G. Kim, S.-G. Kim, G.-S. Park, Y. Kawazoe, H. Lee, Moving beyond bimetallic-alloy to single-atom dimer atomic-interface for all-pH hydrogen evolution, Nat. Commun. 12 (2021) 6766, https://doi.org/10.1038/s41467-021-27145-3.
[35] J.K. Norskov, T. Bligaard, A. Logadottir, J.R. Kitchin, J.G. Chen, S. Pandelov, U. Stimming, Trends in the exchange current for hydrogen evolution, J. Electrochem Soc. 152 (2005) J23–J26, https://doi.org/10.1149/1.1856988.
[36] P. Wei, X. Li, Z. He, Z. Li, X. Zhang, X. Sun, Q. Li, H. Yan, J. Han, Y. Huang, Electron density modulation of MoP by rare earth metal as highly efficient electrocatalysts for pH-universal hydrogen evolution reaction, Appl. Catal. B Environ. 299 (2021), 120657, https://doi.org/10.1016/j.apcatb.2021.120657.
[37] J. Wang, W. Fang, Y. Hu, Y. Zhang, J. Dang, Y. Wu, B. Chen, H. Zhao, Z. Li, Single atom Ru doping 2H-MoS2 as highly efficient hydrogen evolution reaction electrocatalyst in a wide pH range, Appl. Catal. B Environ. 298 (2021), 120490, https://doi.org/10.1016/j.apcatb.2021.120490.
[38] Z.-L. Wang, X.-F. Hao, Z. Jiang, X.-P. Sun, D. Xu, J. Wang, H.-X. Zhong, F.-L. Meng, X.-B. Zhang, C and N hybrid coordination derived Co-C-N complex as a highly efficient electrocatalyst for hydrogen evolution reaction, J. Am. Chem. Soc. 137 (48) (2015) 15070–15073, https://doi.org/10.1021/jacs.5b09021.
[39] Z. Chen, Y. Song, J. Cai, X. Zheng, D. Han, Y. Wu, Y. Zang, S. Niu, Y. Liu, J. Zhu, X. Liu, G. Wang, Tailoring the d-band centers enables Co_4N nanosheets to be highly active for hydrogen evolution catalysis, Angew. Chem. Int. Ed. 57 (2018) 5076–5080, https://doi.org/10.1002/anie.201801834.
[40] D.-R. Deng, F. Xue, Y.-J. Jia, J.-C. Ye, C.-D. Bai, M.-S. Zheng, Q.-F. Dong, Co_4N nanosheet assembled mesoporous aphere as a matrix for ultrahigh sulfur content lithium-sulfur batteries, ACS Nano 11 (2017) 6031–6039, https://doi.org/10.1021/acsnano.7b01945.
[41] W. Zang, T. Yang, H. Zou, S. Xi, H. Zhang, X. Liu, Z. Kou, Y. Du, Y.P. Feng, L. Shen, L. Duan, J. Wang, S.J. Pennycook, Copper single atoms anchored in porous nitrogen-doped carbon as efficient pH-Universal catalysts for the nitrogen reduction reaction, ACS Catal. 9 (2019) 10166–10173, https://doi.org/10.1021/acscatal.9b02944.
[42] W. Wan, C.A. Triana, J. Lan, J. Li, C.S. Allen, Y. Zhao, M. Iannuzzi, G.R. Patzke, Bifunctional single atom electrocatalysts: coordination-performance correlations and reaction pathways, ACS Nano 14 (2020) 13279–13293, https://doi.org/10.1021/acsnano.0c05088.
[43] X. Ao, W. Zhang, Z. Li, J.-G. Li, L. Soule, X. Huang, W. Chiang, H.M. Chen, C. Wang, M. Liu, X.C. Zeng, Markedly enhanced oxygen reduction activity of singleatom Fe catalysts via integration with Fe nanoclusters, ACS Nano 13 (10) (2019) 11853–11862, https://doi.org/10.1021/acsnano.9b05913.
[44] C. Du, Y. Gao, J. Wang, W. Chen, New strategy for engineering hierarchical porous carbonanchored Fe single-atom electrocatalyst and the insights into its bifunctional catalysis for flexible rechargeable Zn-air battery, J. Mater. Chem. A 8 (2020) 9981–9990, https://doi.org/10.1039/D0TA03457F.
[45] A. Zitolo, V. Goellner, V. Armel, M.-T. Sougrati, T. Mineva, L. Stievano, E. Fonda, F. Jaouen, Identification of catalytic sites for oxyge reduction in iron- and nitrogen-doped graphene materials, Nat. Mater. 14 (2015) 937–942, https://doi.org/10.1038/nmat4367.
[46] X. Zhu, X. Tan, K.-H. Wu, C.-L. Chiang, Y.-C. Lin, Y.-G. Lin, D.-W. Wang, S. Smith, X. Lu, R. Amal, N, P co-coordinated Fe species embedded in carbon hollow spheres for oxygen electrocatalysis, J. Mater. Chem. A 7 (2019) 14732–14742, https://doi.org/10.1039/c9ta03011e.
[47] W. Liu, L. Zhang, X. Liu, X. Liu, X. Yang, S. Miao, W. Wang, A. Wang, T. Zhang, Discriminating catalytically active FeNx species of atomically dispersed Fe-N-C catalyst for selective oxidation of the C-H bond, J. Am. Chem. Soc. 139 (2017) 10790–10798, https://doi.org/10.1021/jacs.7b05130.
[48] M. Zhang, Y. Wang, W. Chen, J.-C. Dong, L. Zheng, J. Luo, J. Wan, S. Tian, W.-C. Cheong, D. Wang, Y. Li, Metal (Hydr)oxides@Polymer core-shell strategy to metal single atom materials, J. Am. Chem. Soc. 139 (2017) 10976–10979, https://doi.org/10.1021/jacs.7b05372.
[49] X. Xie, C. He, B. Li, Y. He, D.A. Cullen, E.C. Wegener, A.J. Kropf, U. Martinez, Y. Cheng, M.H. Engelhard, M.E. Bowden, M. Song, T. Lemmon, X.S. Li, Z. Nie, J. Liu, D.J. Myers, P. Zelenay, G. Wang, G. Wu, V. Ramani, Y. Shao, Performance enhancement and degradation mechanism identification of a single-atom Co-N-C catalyst for proton exchange membrane fuel cells, Nat. Catal. 3 (2020) 1044–1054, https://doi.org/10.1038/s41929-020-00546-1.
[50] S. Kunze, P. Grosse, M.T.B. Lopez, I. Sinev, I. Zegkinoglou, H. Mistry, J. Timoshenko, M.Y. Hu, J. Zhao, E.E. Alp, S.W. Chee, B.R. Cuenya, Operando

NRIXS and XAFS investigation of segregation phenomena in Fe-Cu and Fe-Ag nanoparticle catalysts during CO_2 electroreduction, Angew. Chem. 132 (2020) 22856–22863, https://doi.org/10.1002/anie.202010535.
[51] T.A. Smith, J.E. Penner-Hahn, M.A. Berding, S. Doniach, K.O. Hodgson, Polarized X-ray absorption edge spectroscopy of single-crystal Copper(II) complexes, J. Am. Chem. Soc. 107 (1985) 5945–5955, https://doi.org/10.1021/ja00307a020.
[52] Z. Chen, K. Mou, S. Yao, L. Liu, Zinc-coordinated nitrogen-codoped graphene as an efficient catalyst for selective electrochemical reduction of CO_2 to CO, ChemSusChem 11 (2018) 2944–2952, https://doi.org/10.1002/cssc.201800925.
[53] Y. Jiao, Y. Zheng, K. Davey, S.-Z. Qiao, Activity origin and catalyst design principles for electrocatalytic hydrogen evolution on heteroatom-doped graphene, Nat. Energy 1 (2016) 16130, https://doi.org/10.1038/nenergy.2016.130.